SENSITIVITY STUDIES AND LABORATORY MEASUREMENTS FOR THE LASER HETERODYNE SPECTROMETER EXPERIMENT

Frank Allario and Stephen J. Katzberg
Langley Research Center

Jack C. Larsen
Systems and Applied Sciences, Corp.

INTRODUCTION

Several experiments involving spectral scanning interferometers (ref. 1) and gas filter correlation radiometers (ref. 2) using limb scanning solar occultation techniques are currently under development for measurements of stratospheric trace gases from Spacelab and satellite platforms. The scientific requirements for improving the current understanding of the physics and chemistry of the upper atmosphere were recently summarized by several NASA-sponsored science working groups (refs. 3, 4), in which the importance of direct measurements of radical species in the stratosphere were highlighted for the three basic chemical families including chlorine, hydrogen, and nitrogen. Recently, NASA sponsored a science working group to study the role of high resolution spectroscopic measurement techniques in the future development of the Upper Atmosphere Research Program (ref. 5), and emphasized the importance of future collaborative experiments between spectrally scanning interferometers and laser heterodyne spectroscopy techniques from balloon and free-flyer platforms, especially in obtaining simultaneous measurements of a large number of source, sink, and intermediate gas molecules in the stratosphere.

At the Langley Research Center, an experiment to measure stratospheric trace constituents by Laser Heterodyne Spectroscopy has been under study for several years, and a summary of sensitivity analyses and supporting laboratory measurements was recently published (ref. 6). The basic model used for the sensitivity studies included: (1) a line-by-line radiative transfer code to calculate transmission of solar radiation through the upper atmosphere in a limb scanning mode, in narrow spectral intervals (40 to 1000 MHz) spanning the infrared from 2.0 to 15.0 μm; (2) an instrument transfer code to simulate the instrument response function, converting the solar irradiance to digitized voltages as a function of altitude; and (3) an inversion algorithm to convert the digitized voltages to vertical gas concentration profiles. Results were presented for $C\ell O$ and O_3 for a generalized two gas simultaneous LHS experiment.

In this paper, similar sensitivity analyses are presented for O_3, $C\ell O$, and H_2O_2 in which the instrument transfer function is modeled using a detailed optical receiver design currently under study at the Langley Research Center and using recent laboratory measurements of various subsystems of the LHS instrument. The laboratory measurements have been reported in parallel papers at this conference (refs. 7, 8). The spatial frequency response of an LHS-type

Spacelab instrument has also been reported at this conference (ref. 9), and presents results of tradeoff studies performed to achieve a vertical resolution ≤ 2 km and optimum signal-to-noise ratio for the measurement. Results reported in this paper incorporate the results of these other studies and provide performance criteria required for key components of the LHS experiment including the tunable semiconductor lasers, the photomixers, and the pointing and tracking optics. The optical receiver design and supporting analyses and measurements are used to determine projected accuracies for measurement of the vertical profiles of $C\ell O$, O_3, and H_2O_2.

INSTRUMENT TRANSFER FUNCTION (ITF)

ITF Model

The model for the ITF used in the LHS sensitivity analyses is shown in figure 1 and accounts for processing of the input solar radiometric signal and the laser local oscillator through the respective transfer optics, photomixer, wideband preamplifier, five intermediate frequency (I.F.) amplifiers, square law detectors and low pass filters.

The power spectral density of the signal and noise for a given I.F. frequency through the I.F. channelization and amplification stages is given as

$$G_{IF} = e^2 \alpha P_T |H_{PA}(f_o)|^2 |H_{IF}(f)|^2 + \frac{1}{2} \frac{k T_{eff}}{R_m} |H_{PA}(f)|^2 |H_{IF}(f)|^2$$

$$+ e^2 \alpha^2 P_{\ell o} [S^*(f + f_o) + S(f - f_o)] |H_o(f)|^2 |H_{PA}(f)|^2 |H_{IF}(f)|^2 \quad (1)$$

where $S(f - f_o)$ = the spectral power at the photomixer (ergs/sec-cm^{-1}), lower sideband

$S^*(f + f_o)$ = the spectral power at the photomixer (ergs/sec-cm^{-1}), upper sideband

T_{eff} = effective noise temperature of the preamplifier

e = electronic charge

α = η/hf

f = electrical frequency

f_o = local oscillator frequency

η = quantum efficiency

P_T = power required to generate the total shot noise present in the photomixer

R_m = mixer resistance

$P_{\ell o}$ = local oscillator power

$|H_o(IF)|^2$, $|H_{PA}(IF)|^2$, and $|H_{IF}(IF)|^2$ are the power spectral density transfer functions of the photomixer, preamplifier, and intermediate filter/amplifier filter combination, respectively. In the expression for the spectral power density at the photomixer, $S(f - f_o)$, it is assumed that the heterodyne receiver integrates over a solid angle field of view (Ω) and detector area (A), according to Siegman's antenna theorem (ref. 10). The model takes into account appropriate losses due to polarization effects, and chopping of the solar signal (ref. 11), as well as the appropriate optical losses due to the transfer optics. The final output of the signal after the low pass filter is given by

$$G_{LP}(f) = \int_{-B_{LP}}^{+B_{LP}} G_{SQ}(t)|H_{LP}(f)|^2 \, df \tag{2}$$

Assuming $|H_{LP}|^2 = 1$ from $-B_{LP} \leq f \leq B_{LP}$, equation (2) becomes

$$G_{LP}(f) = \left[\int_{-\infty}^{\infty} G_{IF}(\mu) \, d\mu\right]^2 + 2 B_{LP}\left[2\int_{-\infty}^{\infty} G_{IF}(f - \mu)G_{IF}(\mu) \, d\mu\right] \tag{3}$$

The heterodyne signal is then

$$S(I_{DC}) = e^2\alpha^2 P_{\ell o} \, 2\int_{B_{IF}} [S^*(f + f_o) + S(f - f_o)]|H_o(f)|^2|H_{PA}(f)|^2 \, df \tag{4}$$

and the rms noise becomes

$$N(I_{rms}) = \left\{8 B_{LP}\int_{B_{IF}}\left[(e^2\alpha P_T + \frac{k T_{eff}}{2 R_m} + (e^2\alpha^2 P_{\ell o})(S^* + S)|H_o(f)|^2|H_{PA}(f)|^2\right]^2 df\right\}^{1/2} \tag{5}$$

where the IF filter response, $|H_{IF}(f)|^2 = 1$. The first term in equation (5) represents current induced shot noise, the second term describes the thermal noise, and the last term results from the mixing of the noise and signal in the square law device. For the Spacelab experiment, B_{LP} is chosen to filter out as much high frequency noise as possible but still retain sufficient high frequency components of the signal to allow spatial variations in the signal to be measured with a resolution $\leq$ 2 km. In the model, the dc signal currents are assumed to be digitized with a digitization error of ±0.1 percent; the dc signal currents are utilized with the inversion alogorithm to retrieve gas concentration profiles as a function of altitude (ref. 6).

CONCEPTUAL DESIGN OF A TWO-GAS LHS OPTICAL RECEIVER

Optical Receiver

Figure 2 is a schematic diagram of a two-gas simultaneous LHS optical receiver which is currently being used to provide performance criteria for the ITF model. The optical receiver consists of two optical receiver channels in an integrated package, bore-sighted to observe the same tangent altitude in the stratosphere. Functionally, the optical receiver is composed of three basic subsystems including: (1) the transfer optics to simultaneously irradiate the photomixers with the solar and local oscillator (ℓo) radiation; (2) a wavelength identification and control system to identify the frequency of the ℓo to the precision required to invert the radiometric signal, and a microprocessor controlled command system to lock the ℓo wavelength to within 5 MHz (precision) of the center of the absorption line to be measured; and (3) a calibration system with a 1273°K blackbody reference source to provide calibration of the instrument prior to and following measurements performed during the solar occultation measurement period.

The ℓo transfer optics couple the laser radiation to the optical train of the solar signal through either an f/1 germanium lens, or an f/1.5 parabolic mirror at a 50:50 zinc selenide beam splitter. The semiconductor laser is assumed to be completely polarized along the p-n junction (p-type polarization). The transfer optics for the solar radiation consist of a telescope designed to provide a 3-inch collimated beam as the input to the optical receiver. A reflecting beam divider separates the collimated beam into two beams which serve as the input optical trains to the LHS optical receiver. Each optical train is directed to a diffraction grating, blazed to the wavelength of interest and controlled by a shaft encoder with inputs from a central microprocessor system. The diffracted solar signal is focused on the photomixer through two off axis parabolas (f/3) and combined with the ℓo radiation at the Zn-Se beam splitter. The angle of the diffraction grating is set to center the bandpass of solar radiation at the wavelength of the absorption line of the target molecule. Laboratory experiments have been performed to demonstrate that a diffraction grating blazed at the appropriate wavelength (for NH_3, $\nu \tilde{=} 965$ cm^{-1}, 100 grooves/mm) and a bandpass of 1.5 cm^{-1} at the photomixer, yields a spectral rejection ratio of (1000:1) for solar radiation outside the bandpass.

An important design criterion for the optical receiver shown in figure 2 is the lack of a mode rejection system for radiation from the tunable semiconductor laser. This design is based upon results reported by Jäckel and Guekos (ref. 12) in which the high frequency noise intensity spectra from CW GaAlAs semiconductor lasers were studied, and it was generally observed that a lasing mode which is optically isolated from other axial modes of the laser exhibited much stronger intensity fluctuations when compared to the total output of the semiconductor laser, particularly in the frequency range below the intrinsic natural resonance frequency of the laser. Similar noise measurements have been performed with PbSnSe lasers at the Langley Research Center and have been reported at this conference (ref. 7) confirming these conclusions for Pb-salt lasers. Although all Pb-salt lasers which have been tested do not exhibit these noise properties, the number is sufficiently large with present

state-of-the-art lasers to warrant this design. Therefore, in the design shown in figure 2, the solar signal is filtered to a sufficient extent to require the local oscillator to have a mode spacing $\geq 1.5\ cm^{-1}$ in order to confine heterodyning with the solar signal to one axial mode.

In designing the optical receiver in which several modes simultaneously irradiate the photomixer, the added shot noise induced by the extraneous axial modes must be considered in the evaluation of the ultimate signal-to-noise ratio as well as excess noise effects (refs. 6, 7). To minimize effects of the added shot noise on the photomixer current, a requirement must be imposed upon the semiconductor laser which takes into account both excess noise and lack of spectral purity. To develop this requirement, a series of semiconductor laser performance criteria have been generated based upon the following analysis. The signal-to-noise ratio for the heterodyne process can be written as

$$S/N = \kappa \frac{P_S P'_{\ell o}}{2e^2 \alpha P'_{\ell c} + \frac{(F-1)kT_o}{R_m} + 2e^2 \alpha N_e} \tag{6}$$

where $P'_{\ell o}$ = local oscillator power per mode within the bandpass of the filtered solar signal

N_e = equivalent excess noise power

κ = a proportionality factor containing various system constants

P_S = blackbody power

F = noise figure

T_o = $273^{\circ}K$ reference temperature for noise figure

Neglecting the amplifier noise term (second term in the denominator) this equation can be rewritten as

$$S/N = \kappa' \frac{P_S P'_{\ell o}/P_{\ell o}}{1 + N_e/P_{\ell o}} \tag{7}$$

and $\kappa' = \kappa/2e^2\alpha$. If the laser spectral purity is defined as $S_p = P'_{\ell o}/P_{\ell o}$

and the excess noise ratio as $E_{NR} = 1 + N_e/P_{\ell o}$, equation (6) can be written as

$$S/N = \frac{\kappa' S_p}{E_{NR}} = \kappa' F' \tag{8}$$

where $F' = S_p/E_{NR}$ is a figure of merit which defines minimum performance specifications for tunable semiconductor lasers. For a large number of tunable semiconductor lasers which have been tested, the parameter E_{NR} ranged from 1.0 to 1.8 in the quiet regions of the tuning range which for a value of $S_p = 1.0$ results in a typical figure of merit, $F' = 0.55$. This represents a degradation of approximately 0.50 from the theoretically calculated S/N ratio, and is the figure of merit used in the ITF as typical of the expected performance criteria for semiconductor lasers to be used in the optical receiver shown in figure 2. For semiconductor lasers in which the spectral purity (S_p) is <1.0, E_{NR} must be less than 1.8 to maintain a degradation of 0.5 (e.g., for $S_p = 0.8$, $E_{NR} = 1.6$; for $S_p = 0.5$, $E_{NR} = 1.0$). Moreover, by measuring the total laser power of the semiconductor laser, the figure of merit F', and the noise figure of the preamplifier, the expected signal-to-noise ratio for the measurements can be obtained.

In specifying performance criteria for high performance but still practical tunable semiconductor lasers as ℓo's in the experiment, the following criteria are established at the exit window of the cryogenic cooler:

Total Power ≥ 700 μWatts in "P" polarization

Spectral purity ≥ 80 percent in central mode

Mode separation ≥ 1.5 cm^{-1}

$E_{NR} \leq 1.8$

These performance criteria assume the following optical efficiencies in the optical receiver design. Total ℓo radiation losses include the beam splitter (0.5), overfill losses of the ℓo beam image at the photomixer (0.10), and transmission losses of the photomixer window (0.04) for a total transmission efficiency of 43 percent. With 700 μW power at the exit window of the cryogenic cooler, 299 μW of power irradiates the photomixer element which is sufficient to produce 1425 μamps of shot noise current. In the optical train of the solar radiation, optical reflection losses are 0.85 and the loss at the beam splitter is 0.5, for a total transmission efficiency of 0.43. Furthermore, due to the inability to perfectly match the Airey pattern of the solar radiation and the laser ℓo beam, a heterodyne efficiency of 0.84 is assumed in the model. Calculations and trade-off studies performed to optimize the heterodyne efficiency for this design are given in a companion paper to this conference (ref. 9).

Photomixer, Preamplifier, and IF Processing Electronics

The effect of the photomixer, preamplifier, and IF processing electronics on the signal is modeled using power spectral density transfer functions. The

photomixer is modeled using an equivalent electrical circuit (ref. 13) with signal rolloff and shot noise effects included. In the results of the sensitivity analysis reported here, the measured frequency response for photomixer A shown in figure 3 was used from data generated in laboratory experiments (ref. 8). The transfer function was calculated by normalizing curves to a dc value of 1. The shot noise components included in the equivalent circuit are due to the dc current induced by the signal, the local oscillator, and the dark current. In addition, provision was made in the model for a shot noise component induced by excess noise. Noise sources in components following the photomixer are primarily Johnson noise and are combined with the Johnson noise of the photomixer.

The IF processing electronics represent the straightforward application of multipole filters, power distribution amplifiers, and square law RF detection diodes for power detection. The final subsystem in the signal chain is composed of a full-wave synchronous demodulator, running mean integrator and sample and hold circuit. Each element just described was checked to determine fidelity to specification or design and, where necessary, incorporated into the ITF.

Wavelength Identification and Control Subsystem

In figure 2, a wavelength identification and control system is shown in which the laser radiation from the beam splitter is transmitted through an in/out gas cell, a diffraction grating used to isolate the axial mode of the laser which overlaps the absorption line of interest and a 2.5-cm (1-in) diameter in/out Fabry-Perot etalon inserted prior to detection with an Hg-Cd-Te wavelength identification (λID) detector. The primary functions of the wavelength ID and control subsystem are to (1) tune the wavelength of the ℓ_o to the center of the absorption line to an accuracy between 5 to 20 MHz, depending upon the species of interest, (2) provide command and control logic to lock the wavelength to the required accuracy, and (3) provide command and control logic to the cryogenic cooler and laser wavelength drive to utilize a laser operating point free of "excess-noise" effects.

The wavelength ID and control system has been designed to perform identical wavelength calibration functions as used in high resolution spectroscopic measurements of gas molecules (ref. 14), but the control functions in this experiment will be completely automated and controlled by a central microprocessor system. The wavelength ID system is being assembled to perform the following functions in sequence. First, a coarse wavelength selection of the laser mode is performed using a servo-driven grating monochromator at the same time that the solar isolation grating is tuned to the center of the atmospheric absorption line to be measured. A microprocessor system sets the cooler temperature and ramps the injection current to determine operational limits that locate the laser mode within the bandpass of the wavelength identification monochromator. The spectral response of the λID detector is stored by the microprocessor as well as the threshold current I_1 and the current at mode power cutoff I_2. Secondly, the gas cell is driven into the laser beam and the laser signal is ramped again. The reference gas in the cell must be a stable gas with at least two well-known vibration-rotation lines lying on

either side of the atmospheric absorption line to be measured. Suitable reference gases for the 7.5 to 13.0 μm region include OCS, SO_2, and NH_3. The spectral response of the λID detector is again stored by the microprocessor and the two response functions ratioed to obtain the normalized absorption spectra of the reference gas. Third, the Fabry-Perot etalon with free spectral range of 500 MHz is inserted, with the reference gas cell removed, to generate interference fringes to establish the tuning rate for the laser mode. Following this operational step, the microprocessor has sufficient information to set the current of the laser to lock the wavelength near the center of the atmosphere absorption line.

Fine tuning of the ℓo wavelength is achieved by microprocessor interrogation of the five I.F. signal channels to insure during the first solar occultation measurement period that the spectral distribution of the five I.F. channels conforms to expected values. The microprocessor system will be designed to provide this fine tuning capability through control of the temperature and injection current of the semiconductor laser. In the event that the expected absorption line is not identified in the atmosphere, the microprocessor control unit will be placed in a scanning mode of operation to generate absorption spectra of the atmosphere over the tuning range of the TDL mode.

Calibration and Alignment Subsystem

The calibration subsystem shown in figure 2 consists of an 1273°K blackbody source and a collimator assembly unit designed to completely retrace the solar signal through the two channels of the LHS optical receiver, and provides for injection of a highly stable, ruggedized CO_2 laser as a reference ℓo signal to validate performance of the photomixer and the I.F. processing electronics. The calibration system will be used for ground calibration and alignment. A He-Ne laser with a divided two-beam output will be used for ground set-up and alignment (detail not shown on the figure).

LABORATORY MEASUREMENTS

A series of laboratory measurements has been performed to substantiate some of the basic design criteria shown in figure 2 with a laboratory 1-channel LHS instrument. A schematic of the laboratory measurement system is shown in figure 4. The instrument system consisted of three radiation sources including a 1273° K blackbody source, a highly stable CO_2 laser and a tunable semiconductor laser mounted in a standard cryogenic mechanical refrigerator. Experiments were performed in which the blackbody source could be heterodyned with either the CO_2 or semiconductor laser. Similarly, heterodyning experiments have been performed with the CO_2 and TDL lasers. Two photomixers were used in the experiment including a commercial photomixer with a measured effective heterodyne quantum efficiency (η) of 12 percent from 5 to 115 MHz, and a research photomixer with a measured η of 38 percent. The research photomixer was provided by the MIT Lincoln Laboratories, D. L. Spears. Preamplifier noise figures for both photomixers were 2 dB. In general, the laboratory experiments addressed three basic questions:

(1) The signal-to-noise ratio obtained with the tunable semiconductor

lasers when compared to the signal-to-noise measurements obtained with a stable CO_2 laser.

(2) The phenomena of "excess noise" and expected degradations for typical tunable semiconductor lasers either procured under contract, obtained from NASA sponsored research programs,[1] or obtained on consignment from the General Motors Research Laboratories.[2]

(3) The relative magnitude of the RF noise induced by photomixing a multiplicity of axial modes from the tunable semiconductor lasers and the blackbody source and the RF noise induced by a frequency isolated mode from the semiconductor lasers.

In order to determine the projected sensitivity of the LHS experiment to measure trace gas constituents in the stratosphere, laboratory measurements have been performed to compare signal-to-noise ratios with selected semiconductor lasers and highly stable CO_2 laser local oscillators. Figure 5 shows comparative results of the signal-to-noise ratio for measurements with CO_2 lasers (solid lines) and a semiconductor laser (squares). This particular semiconductor laser exhibited nearly single mode output over the current tuning range for a fixed operating temperature. The measured signals for the CO_2 laser measurements were compared to a theoretically derived curve for a 1273° K blackbody, with appropriate losses due to the transfer optics. Comparison between theory and experiment is shown in the figure for the two photomixers. The experiments performed with the semiconductor laser generated a maximum heterodyne detector photocurrent of 400 microamperes (η_{HET} = 38 percent). The higher signal-to-noise ratio for the semiconductor laser results from minor alignment differences and experimental scatter. The important point of these results is that semiconductor lasers, when properly selected for quiet operation, can be as effective as CO_2 lasers in providing signal-to-noise at equal power.

Utilizing the experimentally measured value of 1273° K, the experimental curve was extrapolated to a solar source temperature of 5500° K for an assumed effective heterodyne quantum efficiency of 25 percent and other parameters listed in the figure. These results demonstrate that for semiconductor lasers operating with single mode output, signal-to-noise ratios in excess of 1000 can be achieved using heterodyne detection without requiring the heterodyne photocurrent to be in the shot noise limited regime.

In general, tunable semiconductor lasers operating in a single mode over desired wavelengths for the LHS experiment are difficult to obtain with current technology.

---

[1]Research lasers were obtained from Laser Analytics Incorporated under contract NAS1-15190. Partial funding for this contract was provided by the Los Alamos Laboratories, technical monitor Dr. H. Flicker.

[2]A number of research lasers were obtained from the General Motors Research Laboratories on consignment for test and evaluation in the heterodyne mode. Technical collaborators included Dr. John Hill and Dr. Wayne Lo.

The "excess noise" effects in certain regions have been discussed by Ku and Spears (ref. 15). In a companion paper to this conference, "excess noise" measurements and mechanisms have been discussed (ref. 7). The LHS design shown in figure 2 assumes that semiconductor lasers will be multimode and will operate in the quiet regions of the TDL output. Control of "excess noise" regions by controlling operating temperature and injection current has been discussed previously (ref. 6). In figure 6, comparative measurements of the RF noise power in dB as a function of frequency from 5 to 500 MHz is shown for a typical tunable semiconductor laser and a CO_2 laser local oscillator for a signal induced photocurrent of 400 microamperes. For reference, the preamplifier and dark current noise level for the photomixer and IF processing electronics is shown. As noted earlier, it has been observed that in "quiet" regions of the laser tuning range, the RF noise power can still be more severe for semiconductor lasers than for CO_2 lasers. Measurements were performed using a semiconductor laser in which greater than 80 percent power was in the central mode and the remaining power distributed over three other axial modes. Typical values of the degree to which TDL RF power exceeds that from equivalent CO_2 laser induced RF power are on the order of 2 dB. This residual noise has been used in the ITF in computing the uncertainty in the retrieved concentrations of various trace molecules in the stratosphere using the LHS experiment. For completeness, the measured dependence of the photomixer efficiency as a function of frequency for two photomixers studied in our laboratory is shown in figure 3. In the ITF, photomixer A has been modeled as the expected performance criteria for the LHS experiment.

LHS RETRIEVED CONCENTRATION PROFILES (SIMULATED)

Figure 7 shows results of the LHS sensitivity studies for measuring stratospheric O_3 from Spacelab altitudes, using the ITF function discussed in section 2. For this simulation, an ℓo wavelength at 1129.4420 cm^{-1} was selected to correspond to the peak of a relatively intense O_3 molecular transition lying within an atmosphere window. Five I.F. channels were selected to detect radiances within the O_3 line in order to optimize the sensitivity of the measurement over the entire altitude range. The position of the I.F. channel centers relative to the ℓo wavelength are listed as DNU (cm^{-1}); the bandpass of each channel is listed as BETA (MHz). An integration time, TAU (sec), of 100 ms is used for each channel. For each tangent altitude, two channels are used to invert the radiance data. One channel lies within the O_3 absorption line, and the other channel lies outside the absorption line to account for fluctuations in the background radiance and for continuum absorption effects. For upper altitudes where O_3 attenuation is relatively low, channels near line center are used; for lower altitudes where the O_3 attenuation is high, channels in the wing of the O_3 line are used. The channels selected for various altitudes are listed to the right of figure 7.

In figure 7, the two solid profiles represent the initial and mean retrieved O_3 profile. Error bars indicate ±1 standard deviation of 20 sample retrievals generated by perturbing the simulated instrument current profile with a random Gaussian noise source to simulate random instrument errors. The error bars are an estimate of the uncertainty in the LHS measurement of ozone at various tangent altitudes. Figure 8 shows the fractional error of the

mean mixing ratio for the simulated measurements as a function of altitude for the profile in figure 7. Measurement uncertainties ≤7 percent can be achieved for altitudes ≥20 km. For altitudes below 20 km, the fractional error increases due to the relatively small O_3 concentrations in this altitude range and the large attenuation by O_3 in the outer shells. To obtain a fractional error of the mean ≤7 percent below 20 km requires the use of a second local oscillator tuned to a weaker O_3 transition in order to increase the solar radiance incident upon the Hg-Cd-Te photomixer. Use of two ℓo's for the ozone measurement provide measurement uncertainties ≤7 percent over the total profile.

Figures 9 and 10 show similar results for ClO for an ℓo wavelength of 856.499 cm^{-1} (ref. 16). In figure 9, two retrieved profiles are shown for the same initial profile. In figure 9(a), the conventional inversion algorithm was used as described in (ref. 6). In figure 9(b), a data smoothing cubic spline routine was used to reduce the random errors associated with the retrieved profile. The results show a significant improvement in the retrieved profile where error bars representing ±1 standard deviation are significantly reduced (factor of 6). Although use of the cubic spline technique significantly reduces the error bars, use of the technique will reduce the capability of the experiment to measure spatial variability in the vertical profile for a spatial extent ≤2 km. Figure 10, which shows the fractional error of the mean mixing ratio for ClO, corresponds to the unsmoothed retrieved profiles.

Figures 11 and 12 show similar results for H_2O_2 for an ℓo wavelength of of 1251.2563 cm^{-1}, again for an unsmoothed inversion algorithm.[3] For these simulations, it has been assumed that atmospheric pressure at the tangent altitude can be measured to an accuracy of ±3 percent (ref. 17), and the temperature profile is determined to an accuracy of ±3 K. Results of the studies performed on O_3, ClO, and H_2O_2 with the current ITF indicate the following: O_3 retrievals over the vertical profile from 20 to 50 km can be obtained with accuracies exceeding 93 percent without data smoothing and with accuracies approaching 96 percent with data smoothing; for ClO, accuracies ≥50 percent can be achieved over 20 to 40 km without data smoothing and ≥85 percent with data smoothing; for H_2O_2, accuracies ≥90 and 80 percent can be achieved over 20 to 40 km with and without use of data smoothing techniques, respectively. These sensitivity analyses are currently being conducted for other scientifically interesting gases important to understanding the chemistry of the stratosphere, but depend upon the generation of high resolution spectroscopic parameters including line intensity, line position, and line shapes.

[3] H_2O_2 spectra were provided by Dr. A. Goldman, University of Denver ($\Delta\nu \leq 0.02$ cm^{-1}).

REFERENCES

1. Farmer, C. B.: Infrared Measurements of Stratospheric Composition. Can. J. Chem., 52, 1974, pp. 1544-1559.

2. Russell, J. M., III; Park, J. H.; and Drayson, S. R.: Global Monitoring of Stratospheric Halogen Compounds from a Satellite Using Gas Filter Spectroscopy in the Solar Occulation Mode. Appl. Opt., 16, March 1977, pp. 607-612.

3. Upper Atmospheric Research Satellite Program, Final Report of the Science Working Group, Jet Propulsion Laboratory Publication 78-54, Jet Propulsion Laboratory, Pasadena, CA, June 15, 1978.

4. Chlorofluoromethanes and the Stratosphere. NASA Reference Publication 1010, R. D. Hudson, Editor, Goddard Space Flight Center, Greenbelt, Maryland, 1977, 265 pp.

5. High Resolution Infrared Spectroscopy Techniques for Upper Atmospheric Measurements. Edited by D. G. Murcray and J. M. Alvarez, NASA CP-2134, 1980.

6. Allario, F.; Katzberg, S. J.; Hoell, J. M.; and Larsen, J. C.: An Experiment Concept to Measure Stratospheric Trace Constituents by Laser Heterdyne Spectroscopy. Accepted for Publication in Applied Physics, 1980, Springer Verlag.

7. Harward, Charles N.; and Sidney, Barry D.: Excess Noise in $Pb_{1-x}Sn_xSe$ Semiconductor Lasers. Heterodyne Systems and Technology, NASA CP-2138, 1980. (Paper 10 of this compilation.)

8. Kowitz, Herbert R.: Comparative Performance of HgCdTe Photodiodes for Heterodyne Application. Heterodyne Systems and Technology, NASA CP-2138, 1980. (Paper 22 of this compilation.)

9. Fales, Carl L.; and Robinson, Don M.: Spatial Frequency Response of an Optical Heterodyne Receiver. Heterodyne Systems and Technology, NASA CP-2138, 1980. (Paper 35 of this compilation.)

10. Siegman, A. E.: The Antenna Properties of Optical Heterodyne Receivers. Proc. IEEE, 54, 1966, pp. 1350-1356.

11. Abbas, M. M.; Mumma, M. J.; Kostiuk, T.; and Buhl, D.: Sensitivity Limits of an Infrared Heterodyne Spectrometer for Astrophysical Applications. Appl. Opt., 15, Feb. 1976, pp. 427-436.

12. Jäckel, H. and Guekos, G.: High Frequency Intensity Noise Spectra of Axial Mode Groups in the Radiation from CW GaAlAs Diode Lasers. Opt. and Quant. Electr. 9, 1977, pp. 233-239.

13. Peyton, B. J.; Dinardo, A. J.; Cohen, S. C.; McElroy, J. H.; and Coates, R. J.: An Infrared Heterodyne Radiometer for High-Resolution Measurements of Solar Radiation and Atmospheric Transmission. IEEE Jl. Quant. Elect., QE-11, August 1975, pp. 569-574.

14. Brockman, P.; Bair, C. H.; and Allario, F.: High Resolution Spectral Measurements of the HNO_3 11.3 -μm Band Using Tunable Diode Lasers. Appl. Opt., 17, Jan. 1978, pp. 91-100.

15. Ku, R. T. and Spears, D. L.: High Sensitivity Heterodyne Radiometer Using a Tunable - Diode - Laser Local Oscillator. Opt. Lett., 1977, pp. 84-86.

16. Rogowski, R. S.; Bair, C. H.; Wade, W. R.: Hoell, J. M.; and Copeland, G. E.: Infrared Vibration - Rotation Spectra of the ClO Radical Using Tunable Diode Laser Spectroscopy. Appl. Opt., 17, May 1978, pp. 1301-1302.

17. Park, J. H.; Russell, J. M., III; and Drayson, S. R.: Pressure Sensing of the Atmosphere By Solar Occultation Using Broadband CO_2 Absorption. Appl. Opt., 18, June 1979, pp. 1950-1954.

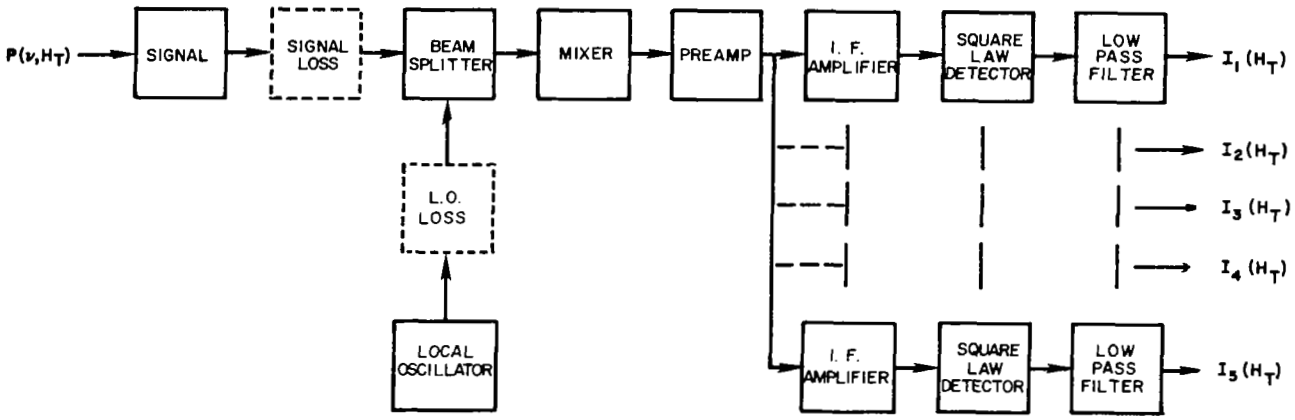

Figure 1.- LHS instrument transfer function model.

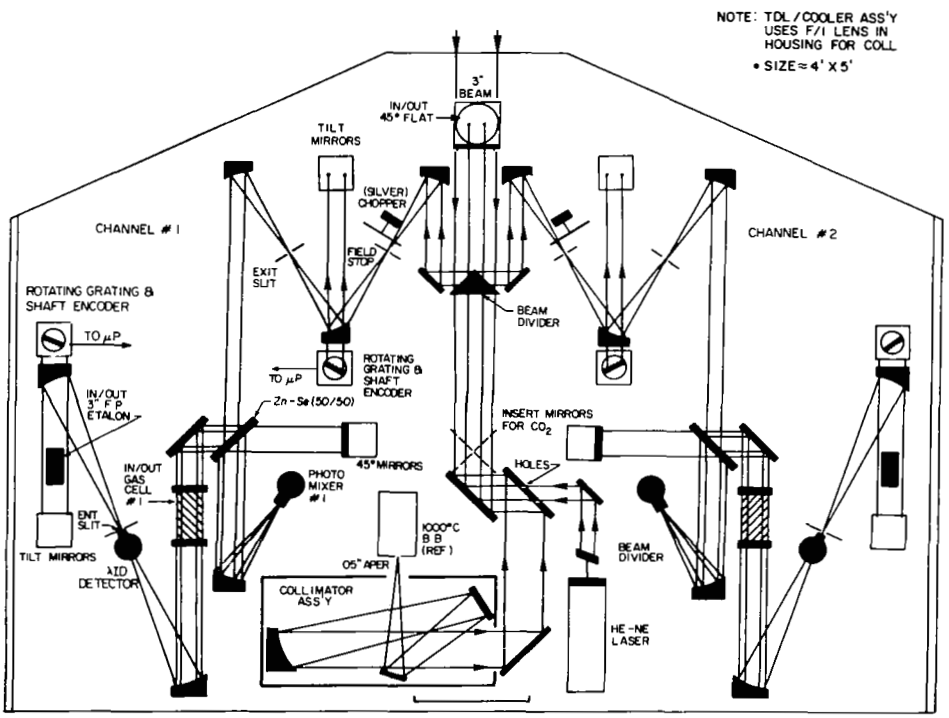

Figure 2.- Schematic of two-gas LHS Spacelab optical receiver.
(1 in. = 2.54 cm; 1 ft. = 0.305 m.)

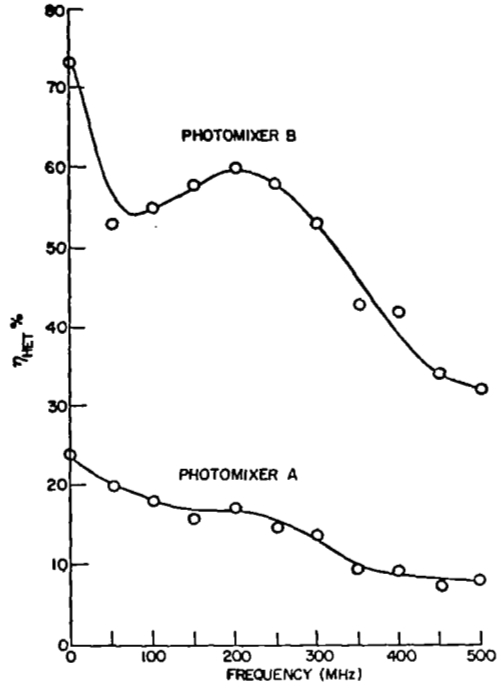

Figure 3.- Measured photomixer quantum efficiency vs frequency. Photomixer A - research photomixer; photomixer B - commercial device.

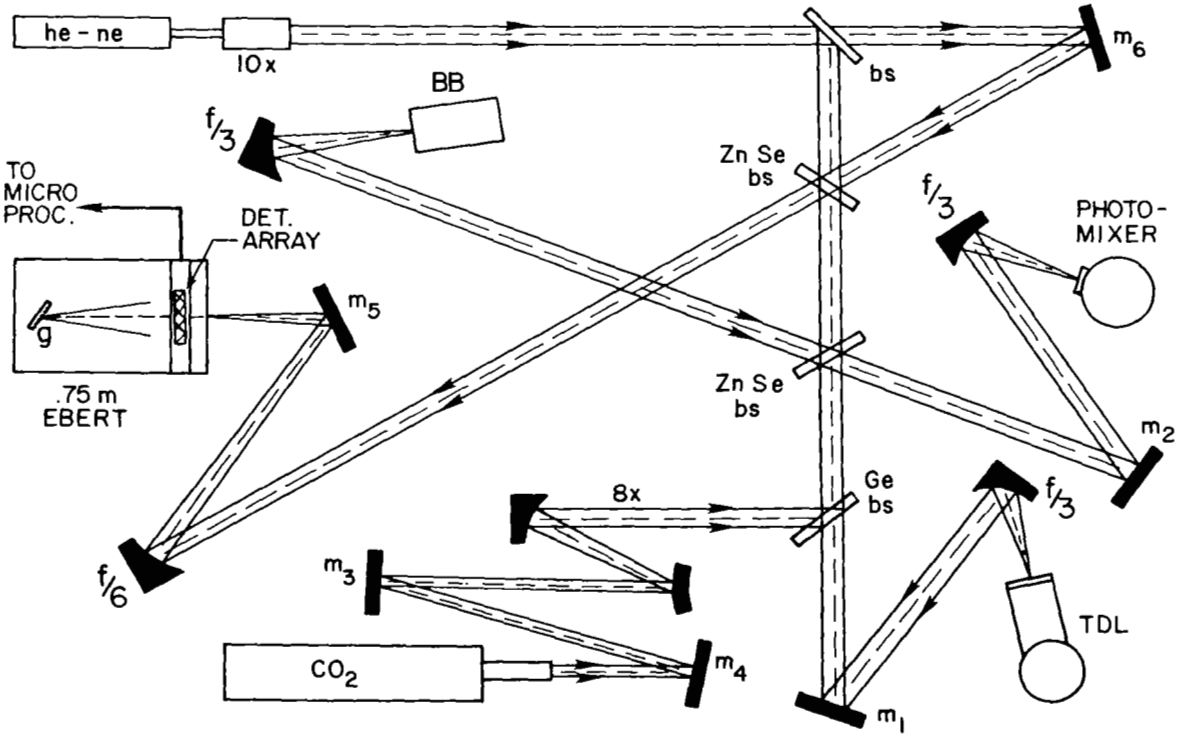

Figure 4.- Single channel LHS laboratory model.

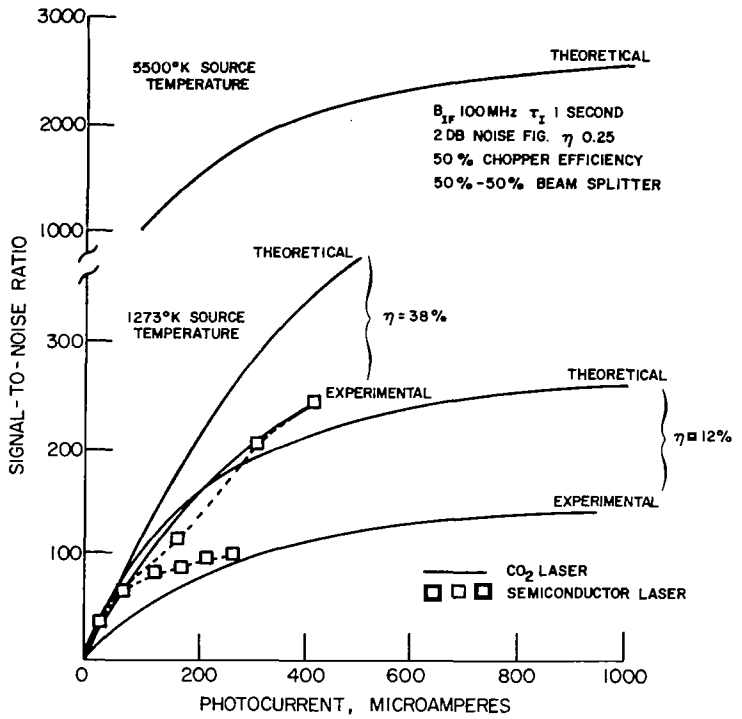

Figure 5.- Comparative signal-to-noise measurements for CO_2 and semiconductor lasers.

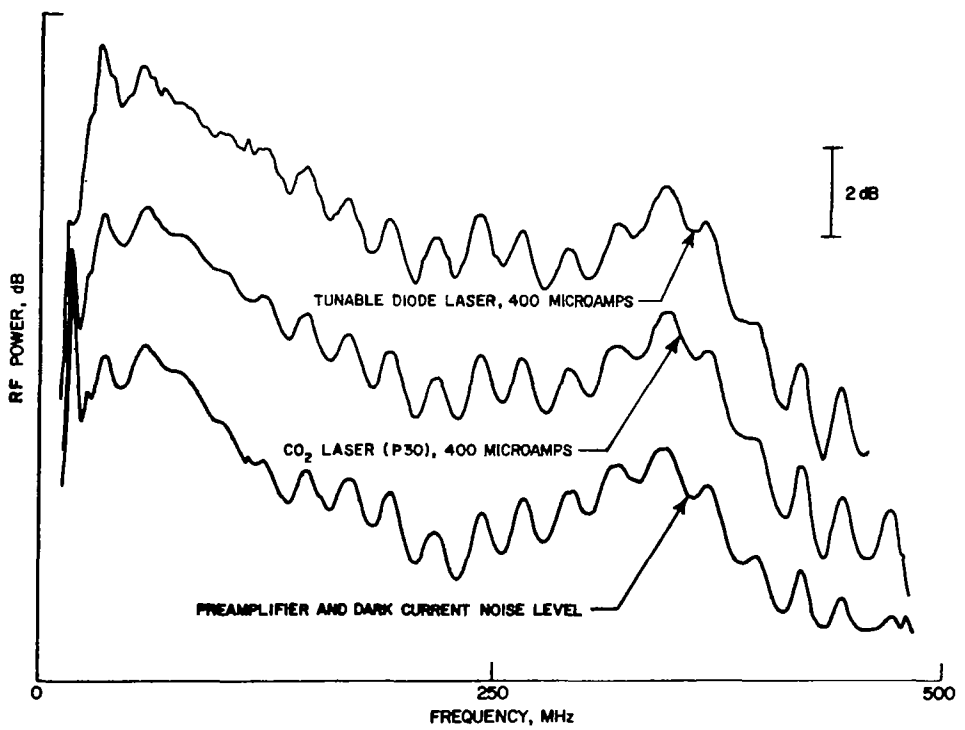

Figure 6.- Comparative RF noise measurements for CO_2 and semiconductor lasers.

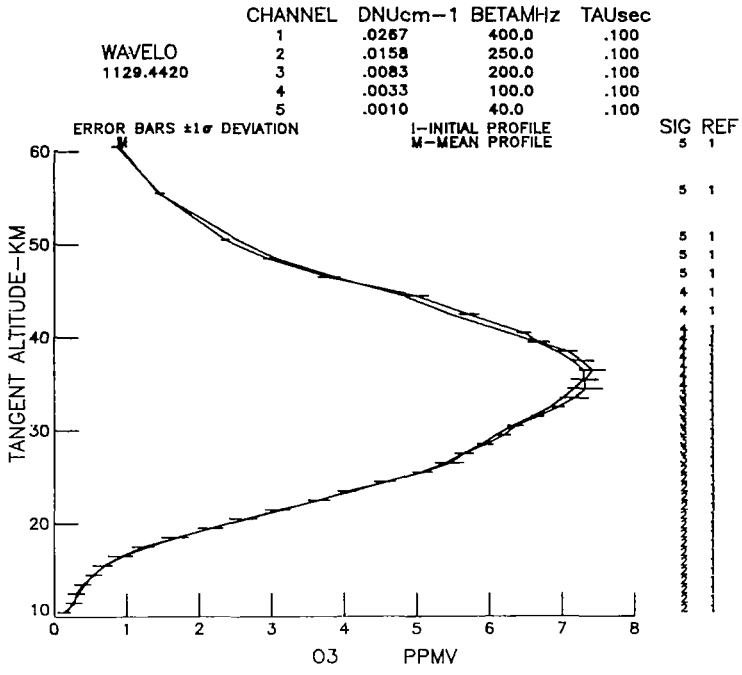

Figure 7.- LHS simulations for stratospheric ozone.

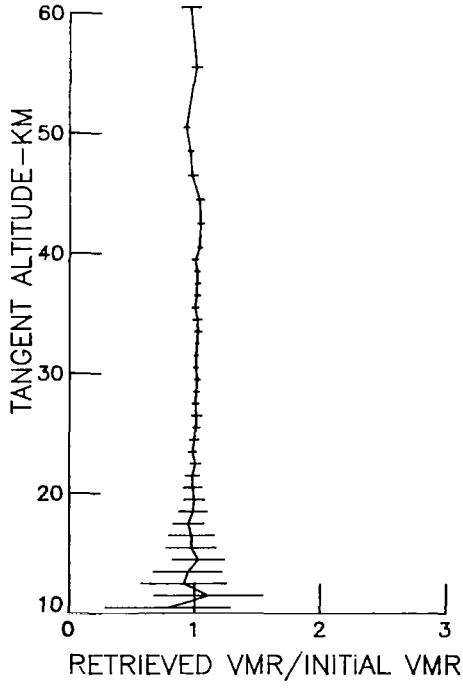

Figure 8.- Fractional error of the mean mixing ratio for O_3. Error bars $\pm 1\sigma$ deviation.

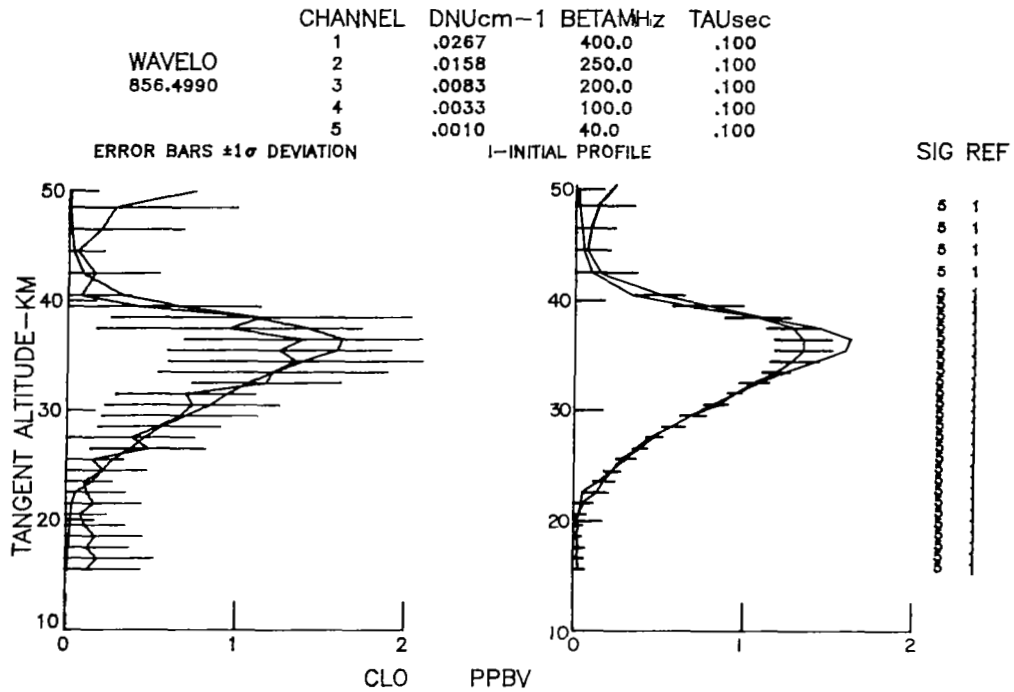

(a).- Without data smoothing (cubic spline technique).

(b).- With data smoothing (cubic spline technique).

Figure 9.- LHS simulations for stratospheric chlorine monoxide.

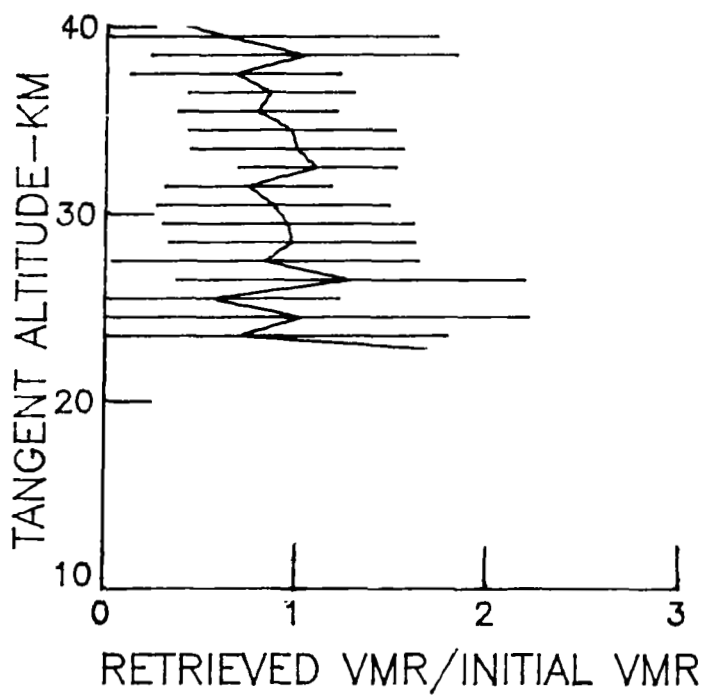

Figure 10.- Fractional error of the mean mixing ratio for ClO. Error bars $\pm 1\sigma$ deviation.

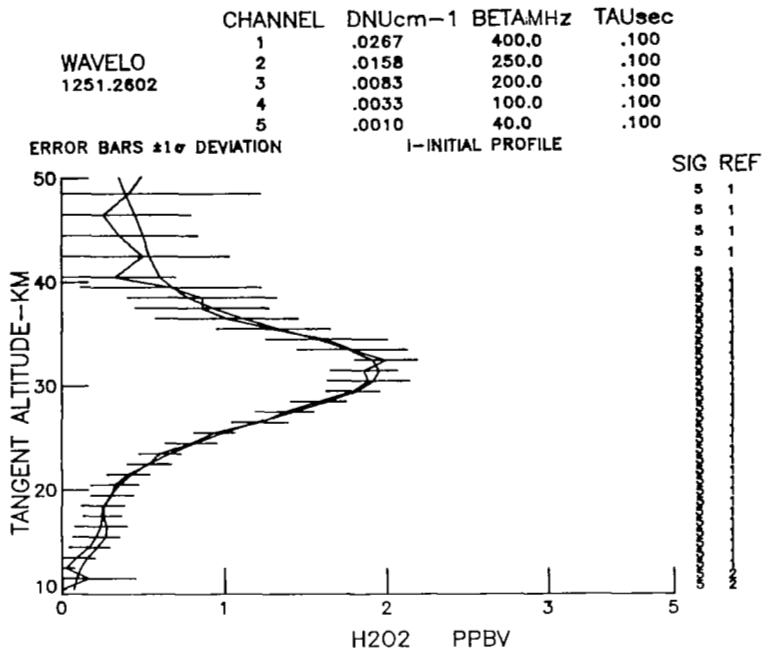

Figure 11.- LHS simulation for stratospheric hydrogen peroxide.

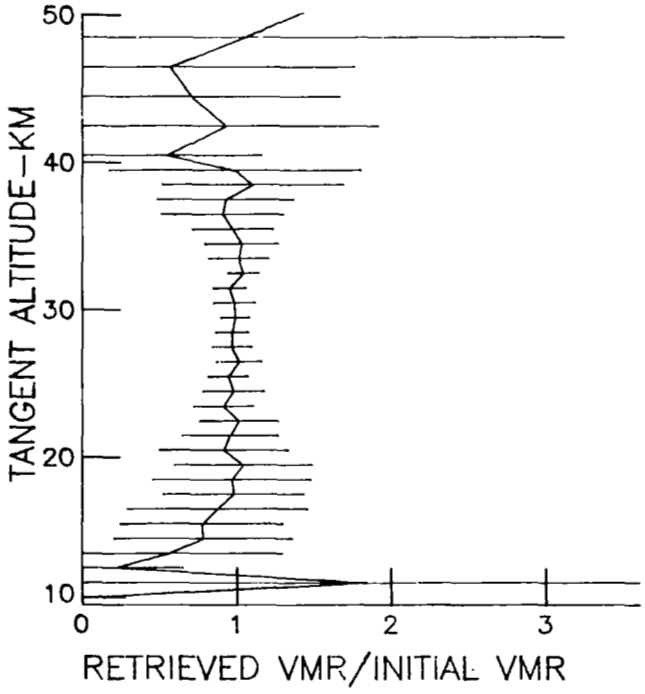

Figure 12.- Fractional error of the mean mixing ratio for H_2O_2. Error bars $\pm 1\sigma$ deviation.